

# Electric-field induced strange metal states and possible high-temperature superconductivity in hydrogenated graphitic fibers

Nadina Gheorghiu\*

UES Inc., Dayton, OH 45432 and

The Air Force Research Laboratory, Wright-Patterson Air Force Base, OH 45433

Charles R. Ebbing

University of Dayton Research Institute, Dayton, OH 45469

Timothy J. Haugan

The Air Force Research Laboratory (AFRL), Aerospace Systems Directorate, AFRL/RQQM, Wright-Patterson AFB, OH 45433

(Dated: January 7, 2022)

In this work, we have studied the effects from increasing the strength of the applied electric field on the charge transport of hydrogenated graphitic fibers. Resistivity measurements were carried out for direct currents in the nA - mA range and for temperatures from 1.9 K to 300 K. The high-temperature non-ohmic voltage-current dependence is well described by the nonlinear random resistor network model applied to systems that are disordered at all scales. The temperature-dependent resistivity shows linear, step-like transitions from insulating to metallic states as well as plateau features. As more current is being sourced, the fiber becomes more conductive and thus the current density goes up. The most interesting features is observed in high electric fields. As the fiber is cooled, the resistivity first decreases linearly with the temperature and then enters a plateau region at a temperature  $T \sim 260 - 280$  K that is field-independent. These observations on a system made out of carbon, hydrogen, nitrogen, and oxygen atoms suggest possible electric-field induced superconductivity with a high critical temperature that was predicted from studying the role of chirality on the origin of life [1].

PACS numbers: 74.81.Bd, 75.50.Dd, 75.70.Rf, 74.50.+r, 74.81.Bd, 74.20.Mn

## I. INTRODUCTION

The role played by pressure on the interlayer coupling effects leading to superconductivity (SC) is by now acknowledged and continues to be intensively explored. For instance, a two-band SC model based on a Ginzburg-Landau free energy with two order parameters can explain how chemical pressure effects can lead to the topological SC in  $\text{MgB}_2$  [2]. In turn,  $\text{MgB}_2$  is considered both crystallographically and electronically equivalent to nonstaggered graphite (the  $\text{B}^-$  layer) that has undergone a zero-gap semiconductor-SC phase transition by large  $c$ -axis chemical pressure due to  $\text{Mg}^{++}$  layers [3]. The application of high mechanical pressure leads to high-temperature superconductivity (HTS) in compounds containing hydrogen (H) ions (hydrides) [4]. High pressure turns the lightest element into a HTS metal [6?] as a result of the Wigner-Huntington transition [7]. H research is also critical for energy storage, rocketry with H as a powerful propellant, and controlled cold fusion.

Recently, flat band SC was found in bilayer graphene twisted at the magic angle  $1.1^\circ$ . The new method - twistronics - can be extended to other 2D correlated electronic states with potential for discovering similar SC materials [8]. While H is the essential component in SC hydrides, controlling the oxygen (O) content in complex oxides can lead to new functional electronic devices [9] as well as SC in cuprates [10].

Recently, several SC features were found for the O-implanted C fibers [11]. As another means for material manipulation, charge injection can lead to new material properties or new heterostructures used for energy storage [12]. Electric fields are a powerful tool used by the semiconductor industry for modulating in a controlled way the charge density in the otherwise insulating metal-oxides. A high enough electric field can lead to a high density of electron-hole pairs or an excitonic Bose-Einstein condensate and thus establish HTS in chalcogenate alloys [13]. The formation of excitonic pairs breaks chiral symmetry and leads to insulating behavior, whereas the formation of Cooper pairs breaks local gauge symmetry and leads to SC. When exploring electric field effects to find new transistors [14], it is important to consider the proximity of SC to metal-insulator (M-I) transitions. Thus, by harvesting pressure (either mechanical or chemical) or/and field effects leads to new SC materials.

The base physical system in this study is the polyacrylonitrile-based (PAN) T300-type C fiber having an average diameter  $7 \mu\text{m}$ . T300 C fibers are usually heat-treated up to  $T = 1500^\circ\text{C}$ , resulting in a graphitized material with a  $\sim 93\%$  C content. The C fiber is turbostratic, with volumes of parallel nearest-neighbor C layers randomly rotated such that the overall structure is random on the small scale and quasi-1D on the fiber's length. The nature of the disorder and its effect on the physical properties of C fibers is not completely understood. Small angle X-ray scattering shows that the C fibers are fractal objects, with their mass scaling relationship given by  $M = L^{d_H}$ , where  $d_H$  is the

\* Nadina.Gheorghiu@yahoo.com

Hausdorff dimension. The scattering intensity for PAN-derived C fibers varies as  $I(S) \propto S^{2.3}$  with  $S$  between 1.5 and  $3 \text{ nm}^{-1}$ , where  $S = \Delta k/2\pi$  and  $k$  is the wavevector. The significantly lower than 3 value of  $S$  mirrors the disordered nature of these C fibers [15]. The room- $T$  thermal diffusivity for these C fibers is the same order of magnitude as in copper,  $D_t \approx (5 - 6) \times 10^{-4} \text{ m}^2/\text{s}$ , thus three orders of magnitude larger than for an YBCO film. In graphite, which is a semimetal, both kind of charge carriers - electrons and holes - are potentially contributing intrinsic charges. Pristine T300 C fibers are characterized by a strongly electronic( $n$ -type) conduction. At  $T = 300 \text{ K}$ , a small input current (few  $\mu\text{A}$ ) results in a  $\rho \approx 1.8 \text{ m}\Omega\cdot\text{cm}$  resistivity, vs.  $\approx 1.7 \mu\Omega\cdot\text{cm}$  for copper. Light-weight (mass density of  $\rho_m = 1.8 \text{ g/cm}^3$  after graphitization) and high-strength material, C fibers have many applications. The tensile strength for PAN T300 C fibers is  $3.6 \text{ GPa}$ , while boron (B) C fibers composites have a Young modulus larger than  $400 \text{ GPa}$ . C fibers are critical material for building space probes like Voyager 1&2. Micro-coiled C fibers, having morphologies very similar to those of DNA, find applications such as electromagnetic wave absorbers or H storage materials [16]. The current density can be as high as  $7.1 \times 10^3 \text{ A/cm}^2$  for silver (Ag)-doped graphene fibers [17] and  $6 \times 10^8 \text{ A/cm}^2$  for copper (Cu)-doped C nanotubes (CNTs) [18], respectively. Hybrid C fiber-HTS materials are used to create stronger, flexible, and chemically stable HTS wires for SC magnets used in particle accelerators, NMR devices or electromagnetic interference shielding covers for spacecrafts. NbN-coated C fibers [19] and YBCO-coated C fibers [20] have critical densities  $J_c$  of the order of  $10^6 \text{ A/cm}^2$  and the upper critical fields  $B_{c2}(0)$  are up to  $25 \text{ T}$  in the former [21]. Improving the flux density pinning in HTS materials is also very important [22] and needs to be considered for each generation of new HTS wires. Attempts are being made for finding SC in C allotropes [23, 24]. The need for decreasing manufacturing costs as well as for guaranteeing material sources leads us to consider more abundant materials when looking for new SC materials.

In this study, we explore the effect of gradually increasing the amount of direct current on the transport properties of octane-intercalated PAN-derived carbon (C) fibers. Resistivity measurements are carried out in the temperature range  $1.9 - 300 \text{ K}$  and for direct currents up to  $14 \text{ mA}$ . The nonlinear nature of the electrical conduction in these C fibers when sourced by high direct currents is analyzed using the Resistor Network (NRRN) model and the Dynamic Random Resistor Network (DRRN) model [26], respectively. The alkane is expected to improve the electronic transport though the free protonation (free  $\text{H}^+$  ions) of graphite's interfaces [27] that can even lead to SC behavior [28]. The presence of O is also expected due to (however small) amounts of water within the fiber. In addition, the fact that this C-H-N-O system has the same elemental composition as the amino acids of life suggests by analogy the possible observation of a similar physical behavior.

## II. EXPERIMENT

Temperature-dependent resistivity  $\rho(T)$  measurements are carried out using a Gifford-McMahon cryocooler, with the vacuum controlled by a Laser Analytics TCR compressor and a Pfeiffer turbo pump. The temperature stabilization is done by a LakeShore 340 Temperature Controller. Current-voltage ( $I - V$ ) measurements are carried out using a Keithley 2430  $1 \text{ kW}$  PULSE current-source meter and a Keithley 2183A Nanovoltmeter. Cryogenic grease [29] assures good thermal contact between the C fiber and the sapphire substrate. Based on known values for the thermal conductivity [30], it is clear that the most significant heat transfer belongs to the C fiber. The sample is placed on the aluminum heater block and four POGO pins [31] are spring-pressed on the fiber. C fibers have anisotropic  $\rho(T)$ -dependence, with the in-plane and out-of-plane  $T$  coefficient of  $\rho$  being  $\alpha_a \approx -3.85 \times 10^{-6} / \text{K}$  and  $\alpha_c \approx 9 \times 10^{-6} / \text{K}$ , respectively. The small change with  $T$  of the ratio between the cross-sectional area and the length of the C fiber,  $S/l$  is neglected. With the system immersed in a cryogenic fluid, the temperature difference between the axis and the surface of the C fiber is given by  $\Delta T = RI^2/(4\pi K_T l)$ . The transverse (along the  $c$  axis) thermal conductivity is  $K_T = 10^{-2} \text{ W}\cdot\text{m}^{-1}\cdot\text{K}^{-1}$ . When a few-mm long C fiber is sourced by  $I \sim \text{mA}$ ,  $\Delta T \sim 1 \text{ K}$ . The effect of a residual resistance is eliminated by using the four-wire Van Der Pauw technique [30], with the  $I$ -to- $V$  gap ratio close to the required factor of four. The quality of the electrical Ag contacts is optically checked using an Olympus B×51 microscope (inset in Fig. 1).

## III. RESULTS AND DISCUSSION

The temperature-dependent resistivity  $\rho(T)$  for raw C fibers is shown in Fig. 1. While one sample (R1) is more resistive, another sample (R2) shows a step-like  $\rho(T)$ . The better conductivity showed by the latter raw C fiber due to a larger amount of incorporated water content. I-M and M-I transitions are observed at  $T \approx 250, 225, 175, 150$ , and  $100 \text{ K}$ , respectively. The multiple-step tunneling feature reflects the existence of abrupt changes in the electric transport (i.e., density of states) at the cooling of the sample. The steps also point to the disordered nature of the graphitic system. As more current is sourced through the fiber, the temperature range where steps in  $\rho(T)$  occur increases. Local maxima in  $\rho(T)$  might also indicate AFM transitions.

While plateau regions in  $\rho(T)$  were also found in closely-packed CNTs film formed by thermal decomposition on SiC and explained on the basis of the STB model [32], the steps between plateaus in  $\rho(T)$  are quite unusual. When the control parameter is the magnetic induction  $B$  instead of the temperature, steps in  $\rho(B)$  are observed with the integer quantum Hall effect as well as fractional quantum Hall effect in graphite [33]-[34]. In the triad  $(\rho, T, B)$ , both  $T$  and  $B$  play

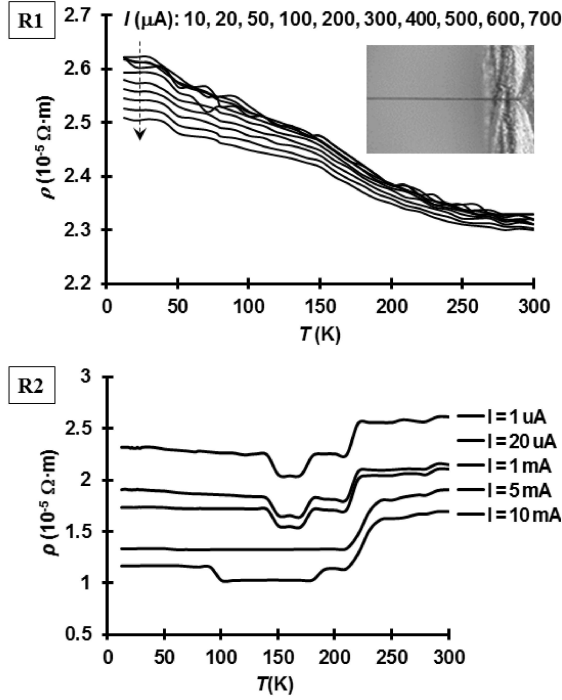


FIG. 1. Temperature dependence of  $\rho(T)$  for two raw C fibers. Sample  $R_1$  is more resistive vs. sample  $R_2$  that shows several I-M and M-I transitions. Inset: Optical microscope image of the  $7\ \mu\text{m}$  in diameter C fiber at one of the (current) Ag contacts.

the role of viscosity in determining the local values of  $\rho$ .

The  $\rho(T)$  landscape for the current density measurements was significantly more richer for the octane-intercalated C fiber. A significant drop in  $\rho$  was found at  $T \sim 280\ \text{K}$ , where the raw C fiber shows only a weak minimum. The minimum in  $\rho$  at  $T \sim 280\ \text{K}$  is consistently observed for all currents (Fig. 2). The current density reaches  $J_c = 3.6 \times 10^4\ \text{A}/\text{cm}^2$  for  $I = 14\ \text{mA}$ . We attribute the difference in the response in  $J$  to the H-rich octane, which can result in the hydrogenation of the  $sp^2$  bonds present in the C fiber and thus improved electrical conductivity. Owing to the existence of Stone-Wales transformation defects, it was found that diamond nanothreads hydrogenated by an organic material such as the hydrocarbon polyethylene becomes less brittle. Although the hydrogenated surface reduces the strength of the Van der Waals interactions, the irregular surface can compensate for the increased interfacial shear strength between the nanothreads and the polyethylene [39]. Likewise, we think that the intercalation of the octane in between the graphite interfaces leads to the formation of hydrogenated  $sp^2$  bonds. The C fibers become less brittle, this benefiting the electronic transport. The metallization of H in the octane-intercalated C fiber is realized in the form of C-H bonds, where the  $\pi$  electrons are like conduction electrons. Then, SC-like states exists locally in complex organic molecules with conjugate bonds [40, 41].

A closer look at the  $I$ -dependent  $\rho(T)$  curves in Fig. 2 re-

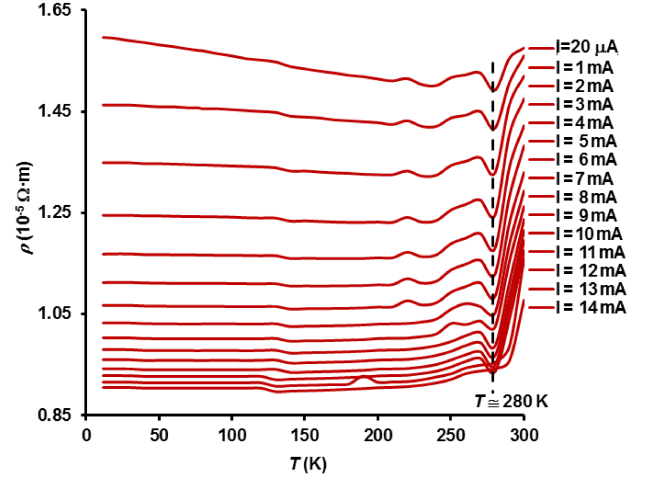


FIG. 2.  $I$ -dependence of  $\rho(T)$  for the octane-intercalated C fiber.

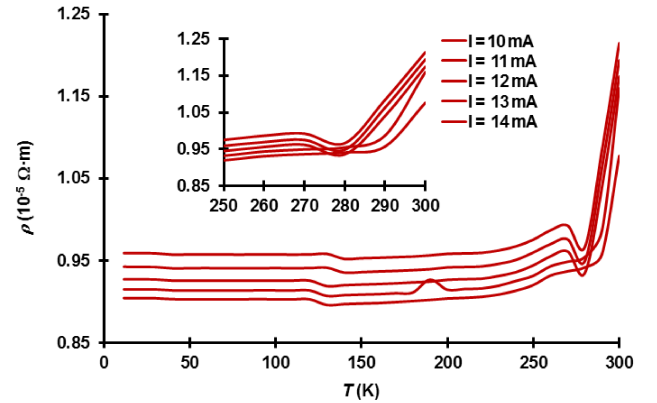


FIG. 3. The high-field effect (i.e., large injection currents) on the  $I$ -dependence of  $\rho(T)$  for the octane-intercalated C fiber.

veals quite an unusual feature. All but two of the curves show a minimum in  $\rho$  at  $T \approx 280\ \text{K}$ . This anomaly was previously observed with PAN-derived C fibers [42]. For  $I < 10\ \text{mA}$ ,  $\rho(T) \sim T$  for  $280\ \text{K} < T < 290\ \text{K}$  and  $\rho \sim T^2$  for  $T > 290\ \text{K}$ . In cuprates HTS, the  $\rho \sim T^2$  dependence in the pseudogap regime coincides with a reduction in the electronic specific heat to a form that is quadratic in  $T$ .  $\rho \sim T$  is the *strange metal* (i.e., normal metal) dependence, which is attributed to the electronic system being well described by the laws of hydrodynamics with minimal viscosity. It results in a linear  $T$ -dependence of the entropy, i.e.,  $\rho$  is proportional to the electronic entropy [43]. The linear  $\rho(T)$  dependence is characteristic to strongly correlated SCs. Twisted bilayer graphene is a spectacular example of a strange metal where the strangeness might entirely result from ordinary electron-phonon scattering. Note that the  $\rho \sim T$  dependence in Dirac systems is independent of carrier density as long as the temperature is

above the Bloch-Grüneisen regime, where  $\rho \sim T^5$  [44]. It has even been argued that strange metals are often in the so-called Planckian limit, where the transport relaxation time is given simply by the temperature  $\tau = \hbar/k_B T$ . For  $T = 280$  K, we find  $\tau \approx 27$  ps. On the other hand, for  $I > 10$  mA, Fig. 3 shows that  $\rho$  first drops linearly with decreasing  $T$  and then for  $I = 13$  mA and  $I = 14$  mA,  $\rho$  almost levels out to a plateau. In addition, the two-step feature in  $\rho(T)$  at  $T \approx 280$  K could indicate the presence of granular SC. While a magnetic field was not applied as in [45], here too we observe an abrupt change in  $\rho$  at the high-temperature, suggesting possible formation of SC crystallites at  $T \approx 280$  K. The following smoother transition at  $T \approx 260 - 270$  K might be due to the existing boundaries between the SC crystallites. Thus, a significant finding here is the linear  $\rho(T)$  feature above  $T \approx 280$  K that suggests a strange-metal behavior. Twisted bilayer graphene with its flat-energy band spectrum is a strange metal, where the linear  $\rho(T)$  (down to  $T \sim 50$  K for higher electron densities) may be arising entirely from ordinary electron-phonon scattering leading to a large electron-phonon coupling constant [44]. In addition, Fig. 3 shows also two small-amplitude transitions: a M-I-M transition at  $T \sim 230$  K and an I-M-I transition at  $T \approx 130 - 140$  K. Notice that extrapolation of the linear  $\rho(T)$  below  $T \sim 280$  K gives  $\rho = 0$  at  $T \sim 160$  K. As mentioned before, the BCS-type mean-field critical temperature for graphene is  $T_c = 150$  K. The linear  $\rho(T)$  extrapolation also gives  $\rho(T = 230 \text{ K}) \approx 0.9 \times 10^{-5} \Omega \cdot \text{m}$ , which is the minimum in  $\rho$  for the plateau region. Within the Planckian dissipative transport [44], where  $\rho \sim mk_B/(n\hbar e^2)$ , we find for the 3D charge density  $\sim 3.6 \times 10^{-19} \text{ cm}^{-3}$ .

The transition at  $T \sim 230$  K is quite interesting, as first-principles calculations predict HTS in metallic H [46]. Correlated fluctuations between electrons and holes that result in the weakening of the Coulomb pseudopotential and band-overlap lead to HTS in molecular H [47], while equal treatment of electrons and phonons result in electron-electron correlations that also lead to HTS [48]. The high- $T$  minimum in  $\rho$  was found at a lower than before, yet close  $T \approx 273$  K for another octane-intercalated C fiber (Fig. 4). As for the plateau feature in  $\rho(T)$ , we find again similarities to the Si-CNTs system mentioned before [32]. Thus, the existence of the plateaus in both the raw and the modified sample are due to the fact that the structural features of the base system, either raw C fiber or pristine CNTs, are invariant.

The percolative nature of the electrical conduction in the octane-intercalated C fiber is evident from the plot of the non-local conductance  $G_{diff}$  at  $T = 130$  K (Fig. 5). As the dc voltage is increased,  $G_{diff}$  (i.e., the slope of  $I(V)$ ) first starts at 1.52 mS, next drops to 0.85 mS, significantly increases to 5.80 mS, and finally goes back to the initial value of 1.52 mS. The high value of 5.80 mS can be explained only by charge tunneling, which results in an increase in the number of conduction channels. The initially low level of the sourced current cannot sustain the feeding of initially percolated channels and the number of percolated channels then decreases. The subsequent increase of the sourced current is enough to

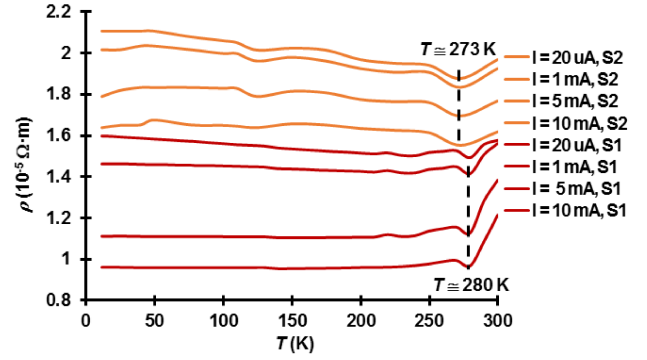


FIG. 4. Comparison between the  $I$  dependence of  $\rho(T)$  for two octane-intercalated C fibers.

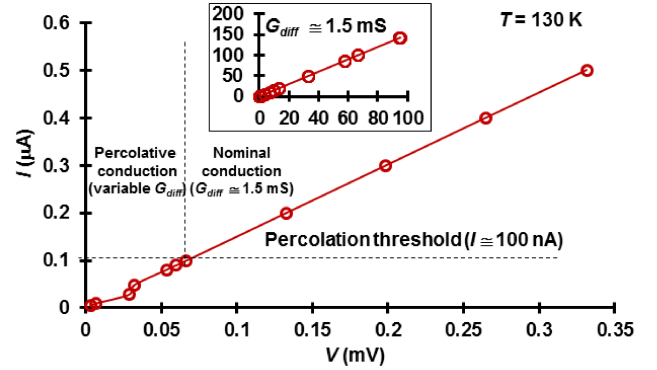


FIG. 5. The percolative (tunneling) nature of the electrical conduction in the octane-intercalated C fiber as revealed by the tuning-like behavior of the slope in  $I(V)$ . The threshold current for setting the nominal regime for electrical conduction through the C fiber is 100 nA.

reestablish the initial number of conduction channels that is given by the electrical conductance of the sample in the nominal working regime, i.e., when the C fiber is sourced by not too low or not too high currents. During this tuning of the electrical conduction, the number of conduction channels varies from  $\approx 39$ , to  $\approx 22$ , to  $\approx 150$ , and back to  $\approx 39$ . The percolation threshold for the sourced current is about 100 nA.

The phenomenon known as electrical percolation is well-known to cause I-M transitions in disordered systems. The charge carriers in a semimetal, electrons and holes, percolate via regions that have a smaller excitation gap  $\Delta E$  between the carriers' energy and the edge of either the valance band (for holes) or conduction band (for electrons) edge. Within the framework of the percolation theory, incremental variation in the number of interconnections present in a random system suddenly causes a long-range connectivity (clustering), resulting in the appearance of a sharp phase transition. The transition from localization to essentially infinite connectivity is similar to a second-order phase transition that can be treated using a scaling (geometrical) construct. Percolation

is basically built into a binary system where the two components have occupied and unoccupied bonds, resulting in the extreme values in the electrical conductance. Of great advantage to finding a solution to the percolation model are two limiting cases: one is a M-I mixture corresponding to  $G_2 = 0$  and the other one is a SC-normal conductor mixture corresponding to  $G_1 = \infty$ . If  $p$  is the volume fraction of either metal or SC, then the composite's macroscopic conductance goes either from zero to a finite value or from a finite value to an infinite value above a percolation threshold  $p_c$ , respectively. The common framework where the percolation phenomenon can be applied to both the I-M and normal-SC transitions suggests the quite entrancing application of the percolation model to the C fibers in this study. The two models used to quantify the physical processes driving the system to a percolative I-M transition are the Nonlinear Random Resistor Network (NRRN) model and the Dynamic Random Resistor Network (DRRN) model [26]. In the NRRN model, the  $I(V)$  relationship is given by:  $V(I) = r_1 I - r_2 I^\alpha$ , where  $r_1$ ,  $r_2$ , and  $\alpha$  are fitting constants. In the DRRN model, there is a power law dependence  $I$  on the electrical conductance (inverse of the resistance)  $G = 1/R$ ,  $I(G) = \beta G^\gamma$ . The major difference between the two models, NRRN and DRRN, lays in the way nonlinearity arrives at the macroscopic scale as a result of electric conduction being networked through the microscopic domains, of the C fiber in this case. In the NRRN model, the nonlinear character of the conduction at the macroscopic scale is a result of the nonlinear conduction in the microscopic elements. In contrast, the DRRN model assumes that the bulk sample can show nonlinear conduction even if the constituent microscopic elements are ohmic resistors. We have applied the two models to the transport data obtained for two C fibers. Results are captured in the table in Fig. 6 and shown in Fig. 7 and Fig. 8 for the NRRN model (a) and the DRRN model (b), respectively. Clearly, the NRRN model is a better fit to the experimental data for the octane-intercalated C fibers. Others found that the DRRN model better describes thin gold films near the percolation threshold [49]. The important conclusion here is that the electrical conduction is nonlinear at all scales of the octane-intercalated C fiber. This was actually expected, as the localization length  $a^{-1}$  cannot possibly be a match to the diameter of the C fiber. Thus, the  $V(I)$  dependence for the octane-intercalated C fiber is non-ohmic and it has a  $I$ -dependent shape (Fig. 7).

One important quantity characterizing the electronic transport through wires, in this case the C fibers, is the current density  $J$ . Solving  $V(I) = r_1 I - r_2 I^\alpha$  for  $I$ , we find that  $V = 0$  (except for  $I = 0$ ) for  $I = 0.4$  A and  $I = 0.1$  A for the two octane-intercalated C fibers denoted here by S1 and S2, respectively. The observed nonlinear electrical conduction results in decreasing  $\rho$  with increasing the sourced current density  $J = I/S$ , as Fig. 9 shows. For  $I \geq 1$  mA, there is a good agreement between experimental data for the octane-intercalated C fiber and the NRRN model, manifested in the monotonic decrease of  $\rho$  with  $J$ . The most likely cause for the non-ohmic character of the conduction observed with

Carbon fiber sample	Fit to the NRRN model $V(I) = r_1 I - r_2 I^\alpha$			Fit to the DRRN model $I(G) = \beta G^\gamma$	
	$r_1$ ( $\Omega$ )	$r_2$ (V/A $^\alpha$ )	$\alpha$	$\beta$ (A/S $^\alpha$ )	$\gamma$
S1	1350	1600	1.18	$5.10 \times 10^8$	5.88
S2	1088	5969	1.73	$2.06 \times 10^{16}$	6.29

FIG. 6. Results of fitting transport data for octane-intercalated C fibers to the NRRN model and DRRN model, respectively.

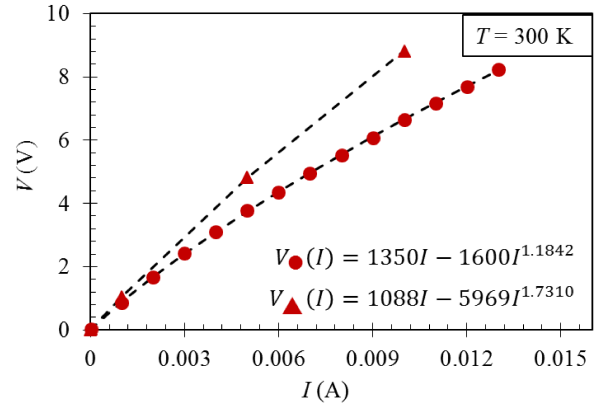


FIG. 7.  $I(V)$  experimental data for two octane-intercalated C fibers and the fit to the polynomial functional  $V(I)$  from the NRRN model,  $V(I) = r_1 I - r_2 I^\alpha$ .

the application of high electric fields is the field-induced tunneling.  $\rho$  would be ideally zero or practically negligible (i.e., as for a SC) at  $J_c \approx 1.0 \times 10^6$  A/cm $^2$  for the lower-resistance octane-intercalated C fiber (sample S1). While it is surprising to find that  $J_c$  found here is close to the one for HTS materials, clearly the C fiber would never reach such high  $J$  due to the extreme heating effects. Though the linear increase  $\rho(T)$  above its minimum is primarily an indicative of the two-dimensional (2D) weak localization, a well-known linear dependence is also observed in HTS materials above their critical temperature  $T_c$  [50].

The  $I(V)$  data for  $T = 130$  K plotted as nonlocal differential conductance  $G_{diff} = dI/dV$  (Fig. 10) shows two minima at voltages  $V \approx 0.06$  mV ( $eV \approx 0.096$  meV) and  $V \approx 63$  mV ( $eV \approx 101$  meV).

At larger voltages,  $G_{diff}$  has a monotonic increase due to percolative conduction. As known,  $G_{diff}$  shows minima at voltages  $\Gamma/|e|$  ( $e$  is the electron's charge), where  $\Gamma < \Delta < G$ , with  $\Gamma$  the exciton superconducting gap,  $\Delta$  the superconducting gap, and  $G$  the overlap band gap [51]. Such minima are seen as a hallmark of the existence of the gaped excitonic state. The second minimum here would give a BCS critical temperature  $T_c \approx 2\Delta/k_B > 2\Gamma/6k_B \approx 244$  K. The value of the gap ratio  $2\Delta/k_B T_c$  considered here is at least 6, as pre-



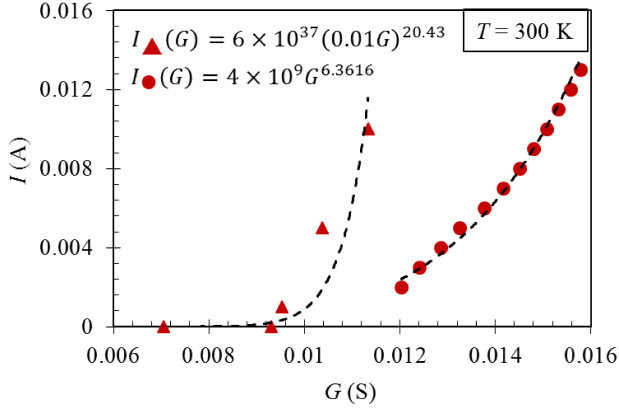


FIG. 8. Nonlinear current-dependent conductance experimental data for two octane-intercalated C fibers and the fit to the power law dependence  $I(G) = \beta G^\gamma$  from the DRRN model.

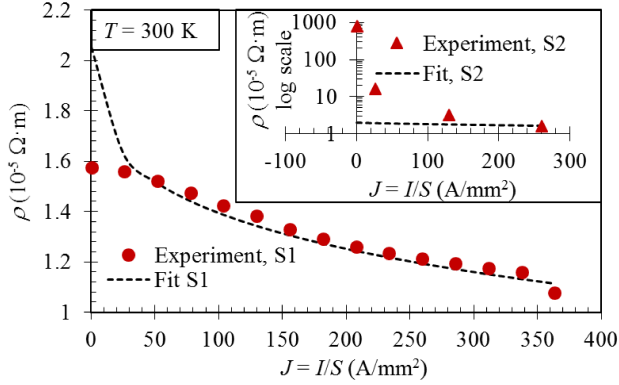


FIG. 9. Resistivity-current density  $\rho(J)$  experimental data for two octane-intercalated C fibers at  $T = 300$  K. Also shown is the fit to the dependence derived from the NRRN model,  $\rho(J) = r_1 - r_2 J^{\alpha-1}$ .

viously obtained from the large gap value in [52]. On the other hand, the significant drop in  $\rho$  at  $T \approx 280$  K suggests that if this would be in fact  $T_c$ , then the corresponding gap ratio would need to be 6.9. In any case, the high value of the gap ratio clearly suggests the unconventional nature of SC in these hydrogenated C fibers. This would also give pairing energy  $\Delta_{pair} \approx 1.3 \times \Delta > 1.3 \times 101 \text{ meV} \approx 131 \text{ meV}$  (or 364 K, close to temperature for bipolaron decay in Poly A/ Poly T DNA duplexes [73]). Notice that for single-walled CNTs, the energy gap obtained from tunneling measurements is around  $\Delta \approx 100 \text{ meV}$  [53]. We also find for the exciton frequency is  $f = 2|e|\hbar \approx 31 \times 10^{12} \text{ Hz} = 31 \text{ THz}$ , where  $\hbar \approx 6.62 \times 10^{-34} \text{ J}\cdot\text{s}$  is Planck's constant. The corresponding wavelength  $\lambda = c/f \approx 10 \mu\text{m}$  is of the order of the fiber's diameter  $d = 7 \mu\text{m}$  ( $c \approx 3 \times 10^8 \text{ m/s}$  is light speed in vacuum). Note that THz spectroscopy is used to analyze Higgs bosons, i.e., collective modes in multiband SCs like  $\text{MgB}_2$  [54] and hydrogenated graphitic fibers [11, 52].

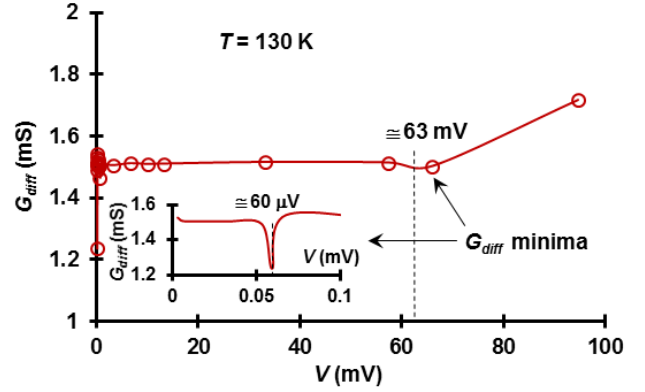


FIG. 10. Nonlocal differential conductance at  $T = 130$  K. Two local minima are observed, with the one at the higher voltage possibly caused by the existence of interfacial SC currents that result in a THz wave emission.

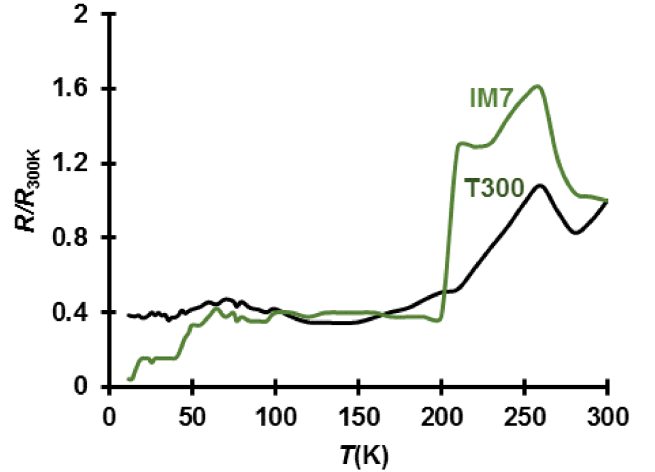


FIG. 11. Temperature dependence of the resistance (relative to room-temperature resistance) for bundles of C fibers T300 ( $N = 1000$ , in black) and IM7 ( $N = 12000$ , in green) sourced by  $I = 20 \mu\text{A}$  direct current.

I-M transitions were also observed in bundles of raw C fibers, T300 type (1000 C fibers), and IM7 type (C content 95%) are shown in Fig. 11. Importantly, the in-plane mean free path of electrons becomes equal to the C fibers diameter when the latter is  $d \leq 5 \mu\text{m}$ , a condition that is marginally fulfilled by the IM7 C fiber ( $d = 5 \mu\text{m}$ ). The resistance was plotted relative to the room-temperature value. There are several I-M transitions: a significant one at  $T \approx 260$  K, close to the one found for single C fibers, at  $T \approx 220$  K, and at  $T \approx 60$  K. Again, the latter occurs at the mean-field predicted temperature for SC correlations. The IM7 also shows the better-known I-M transition at  $T \approx 25$  K. With all these I-M transitions, the resistance changes in an almost step-like manner. As the presence of small amount of  $\text{H}_2\text{O}$  cannot be ruled out,

we also notice that  $T = 25$  K is the ice point for CO. Recently, it was found that all comets originate from the same point in the Universe based on the vicinity to the CO iceline in time [55]. It is not unreasonable to assume that material properties, in particular for C allotropes, can be traced to past physical processes in our solar system. It was also found that the grain-surface chemistry is mainly driven by hydrogenation reactions leading to high abundances of  $\text{H}_2\text{O}$ ,  $\text{CH}_4$ ,  $\text{C}_2\text{H}_6$ , and  $\text{CH}_3\text{OH}$  ices. We also observe that the plateau feature in the  $\rho(T)$  dependence is even more similar to the case of Si-CNTs system mentioned before, when comparing the C fiber bundles here to the closely-packed CNTs [32]. In addition, the plateau in  $\rho(T)$  is centered at  $T = 150$  K. In graphene, BCS-type SC with a mean-field critical temperature as high as  $T_c = 150$  K was calculated for an electron density (2D)  $n = 10^{14} \text{ cm}^{-2}$  and it was explained as a Cooper-like pairing instability owing to a more efficient Coulomb screening [56]. The metallic-like behavior observed with these bundles of C fibers, particularly the one below  $T \approx 260$  K, can be the result of parallel contributions to the electrical resistance of neighboring interfaces (graphene planes). Significantly, granular SC might be found at the embedded interfaces [57, 58]. On the other hand, the I-M transition occurring at  $T \sim 260$  K might have a special nature. Possible products of the heat treatment/carbonization used in the making of C fibers are the  $\text{C}_{60}$  (fullerene) clusters. Moreover, the ion-implantation process can fragment these large C molecules. In any case, let us assume that the C fiber contains large C molecules, with  $\text{C}_{60}$  among them. At room temperature, the pure  $\text{C}_{60}$  crystal adopts a face-centered cubic structure. The molecules freely rotate with respect to each other and orientational disorder reigns. Then, below  $T \sim 260$  K, electrostatic interactions between electron-poor ( $p$ -type) and electron-rich ( $n$ -type) regions of neighboring molecules results in a freezing of the free molecular rotation. In this rotation-free state, the four molecules of the face-centered cubic unit cell become orientational non-equivalent and the  $\text{C}_{60}$  undergoes a first-order phase transition to a simple cubic crystal structure [59, 60]. Structural phase transition at a higher temperature precedes the charge density wave order occurring at a lower temperature in the SC state. Thus, the structural transition at  $T \approx 260$  K is followed by a series of steps in  $\rho(T)$  with the one occurring at  $T \approx 60$  K. HTS in YBCO thin films and fullerenes was previously attributed to percolative conduction between clusters [61]. Metallic cluster-based SC tunneling in Josephson-linked networks, for which the presence of electronic energy shells is similar to those in atoms and nuclei, is the key ingredient to finding room- $T$  SC [62]. Moreover, the fullerenes can also encapsulate the H under enough pressure and the short-range order instability suggests a two-fullerene cluster unit with the SC metallic  $\text{H}_2$  resulting from having a H atom inside each fullerene. Indeed, extrapolating the experimental  $T_c(\sqrt{M})$  plot in Fig. 4 from [61] ( $M$  is the cluster mass in atomic units  $m_u \approx 1. \times 10^{-27}$  Kg), we find that a  $T_c \approx 50$  K would correspond to a mass of about  $1600m_u = 133m_C$ , with  $m_C$  the mass of a C atom. I.e., this could be the mass of a two-

fullerene dumbbell cluster with a H atom inside each fullerene molecule. The role of O, either implanted [11] or trapped (and under compressive stress along the crystallographic  $a$ -axis) [63], cannot be excluded when discussing the observed I-M transitions.

#### IV. CONCLUSIONS

In this work, we have studied the effects of stepping up the strength of the applied electric field on the charge transport of hydrogenated graphitic fibers. We have found that the conduction has a percolative nature that is better described by the NRRN model than by the DRRN model, suggesting that the fiber is nonlinear at all scales, possibly benefiting the occurrence of SC fluctuations in this graphitic system. The percolation model was recently applied to cuprates, where it was found that the superconducting precursor is strongly affected by intrinsic inhomogeneity [64]. The (spatial) nonhomogeneous nature of the SC gap in cuprates is reflected in the distribution of local transition temperatures and thus naturally leads to percolation. It might be also the case with the C fibers here, as percolation comes naturally to these fractal objects. Percolation is also needed if assuming that SC is the primary state at “generic” incommensurate fillings and is being “interrupted” by insulating states at the commensurate fillings [65]. The self-organized percolative, filamentary, nature of SC in these systems might be actually captured at their room- $T$  preparation, thus HTS is inserted in fractal systems by design. In ferromagnetic SCs, self-organization appears to be the main mechanism responsible for filamentary SC by minimizing the dopant-related free energy at the formation  $T$  [66]. The observed electric field-induced tunneling suggests possible existence of Josephson grain-coupling in these C fibers. The temperature-dependent fiber’s resistivity  $\rho(T)$  shows several SC-like features: step-like transitions between insulating and metallic states, plateau regions, and high- $T$  strange metal behavior as a hallmark of non-Fermi liquid with strong electron correlations and where nematic fluctuations are important. The interplay between disorder and SC fluctuations results in linear  $\rho(T)$  at the I-M transition points. Defects lead to weak localization, which favor electron-electron localization and hence SC correlations. Increased charge injection remove some of the defects and thus leads to a decrease in the electrical resistance. The low- $T$  resistivity is plateaued to a finite value, resembling the saturated  $\rho(T)$  for thin SC films that is due to either vortex depending or overheating effects [36]. Compared to the raw graphitic fibers, the plateaus for the hydrogenated fibers are extended over larger temperature intervals suggesting a clearly more metallic behavior. As known, thermal fluctuations at the SC grain boundaries lead to: a) the activation of vortices as explained by Tinkham [37] and b) a loss of phase coherence across the Josephson junction accordingly to the model by Langer, Ambegaokar, McCumber, and Halperin (LAMH) [38]. In both cases, a  $2\pi$  phase slip occurs resulting to the step-like, i.e. abrupt change in

temperature dependence of the electrical resistance.

We believe that this work is contributing to the growing evidence of SC located at graphite interfaces, in particular after the samples were brought in contact with alkanes [27]-[28], [67]. The octane intercalation increases the carrier concentration in graphite and it was found to play a crucial role in inducing interfacial SC through the formation of Josephson junctions within the sample. The H-rich alkane might lead to the formation of ferrimagnetic puddles within the sample. Possible coexistence of SC and magnetism at the interfaces of graphite that had undergone certain modification processes, as suggested by [75], was indeed found [11, 52]. It was suggested that in order to reach room- $T$  SC, one must search for or artificially create systems that experience the nontopological flat band in the bulk or topologically protected flat bands on the surface or at the interfaces of the samples [68]. Within mean field approximations, it is shown that chiral SC domains are naturally induced by the ferromagnetic domains [76]. At their grain interfaces, these hydrogenated graphitic fibers might be harboring both FM-SC-FM spin valves and Josephson junctions.

The I-M transition at  $T \sim 260 - 280$  K might be related to *chirality*, perhaps the most fundamental property in nature. Owing to the presence of spin carrying protons  $H^+$  introduced by the intercalation with an alkane, it is possible that the octane-intercalated C fiber is a chiral ferromagnetic SC. This leads us to a much relevant connection. The molecules of life, the DNA and RNA, are chiral and their liquid crystal nature has been researched [69, 70]. Chirality can also be found in graphitic materials. For instance, if one rolls up a graphene sheet along the  $a$ -axis, a zigzag nanotube is obtained. By rolling a graphene sheet in the direction  $\theta = 30^\circ$  relative to the same axis, an armchair nanotube is obtained. For  $0^\circ < \theta < 30^\circ$ , a nanotube called chiral will be formed. While the PAN C fiber has a turbostratic structure, one thing in common with the DNA is the presence of elements H, N, C, and O. Interestingly, taking into account the old ages of eucrite meteorites and their similarity to Earth's isotopic ratios of H, C, and N, it was demonstrated that these volatiles could have been added early to Earth, rather than gained during a late accretion event [71]. Even more significantly, these elemental atoms are also present in the amino acids that compose the DNA molecule. Early studies on double-stranded DNA found that delocalized  $\pi$  electrons lead to room- $T$  SC-type behavior [72]. Bipolaron HTS in Poly A/ Poly T DNA duplexes was found to decay at about 350 K, which can be taken as approximate estimate of  $T_c$  [73]. While the alkane turns the graphite from hydrophilic to hydrophobic [74], the water can still be readily adsorbed in some regions of the C fiber, thus the presence of O. In the '90's, Salam suggested that biomolecular homochirality that originated with Pasteur can be achieved through a phase transition: the D-amino acids would change to L-amino acids as the  $C_\alpha$ -H bond would break and the H atom would become a superconductive atom [1, 77]. The 'D' and 'L' here stand for the right and left mirror sym-

metry, respectively. Salam estimated the transition temperature to  $\sim 250$  K and possibly even above 350 K. We think that it might not be a mere coincidence with the case of octane-intercalated C fibers here, where an I-M transition occurs persistently at  $T \sim 260 - 280$  K for different fibers and regardless of the amount of sourced current. Fig. 11 shows that the I-M transition at  $T \sim 260 - 280$  K is also observed for bundles of raw C fibers. The O and the H atoms would be likely brought by any small amount of water retained by the C fibers during their preparation. Real-space molecular-orbital density-wave description of Cooper pairing in conjunction with the dynamic Jahn Teller mechanism for HTS predicts that electron-doped water confined to the nanoscale environment of a C nanotube or biological macromolecule should superconduct below and exhibit fast proton transport above the transition temperature,  $T_c \approx 230$  K [78]. Electrocrystallization of supercooled water confined by graphene walls was also found [79] at  $T \approx 268$  K, close to the notable temperature for the C fibers here. The linear size of the water confinement in [79] is 100 Å, which happens to be also the length of relatively straight domains in C fibers. Remarkable, the formation and evolution of biological structures occurred where both carbon and water were present. More than a mere imperfection, the water retention was crucial for the formation of life. Rosalind Franklin and her colleagues showed that DNA formed a helix conforming to the one modeled by Watson only within a limited yet precisely *designed* range of humidity [80]. Is it possible that the phase transition that created the helical structures of DNA and RNA and the one Salam refers to as superconducting and occurring around the room temperature are actually the same thing? Worth mentioning is one particular property of hydrogen-modified graphene to behave as a shape-changing membrane [81] is essential to its relation to amino acids and the SC transition at 250-300 K predicted by Salam.

Hydrates-based SC in microtubules could be responsible for quantum processing of information, such that the unprecedented computational power of the brain might actually come from its superconducting nature [82]. The  $T_c \sim 2000$  K there is close to our previously find maximum  $T_c \sim 2360$  K [52], which in turn is close to Little's early 1964 prediction for superconductivity in linear chains of organic molecules linked to certain molecular complexes [83], also close to Schrieffer's prediction for exotic HTS [84]. There are clear implications related to the coherent nature of the brain, its long-term memory, and human subconsciousness. *It is possible that superconductivity is organic to the living matter.* The topic needs more attention and resources, as it is as of paramount importance both fundamentally and for unforeseen applications.

#### ACKNOWLEDGMENTS

This work was supported by The Air Force Office of Scientific Research (AFOSR) LRIR #14RQ08COR and & LRIR #18RQCOR100 and the Aerospace Systems Directorate (AFRL/RQ). We acknowledge J.P. Murphy for the cryogenics. Special gratitude goes from the first author to Dr. G.Y. Panasyuk for his continuous support and inspiration.



- 
- [1] A. Salam, J. Mol. Evol. **33**, 105 (1991).
- [2] J.J. Betouras, V.A. Ivanov, and F.M. Peeters, Eur. Phys. J. B **31**, 349 (2003).
- [3] G. Baskaran, Phys. Rev. B **65**, 212505 (2002).
- [4] L.P. Gor'kov and V.Z. Kresin, Rev. Mod. Phys. **90**, 011001 (2018).
- [5] N.W. Ashcroft, Phys. Rev. Lett. **21**, 1748 (1968).
- [6] E. Babaev, A. Sudb, & N. W. Ashcroft, Nature **431**, (2004).
- [7] E. Wigner and H.B. Huntington, J. Chem. Phys. **3**, 764 (1935).
- [8] S. Carr, S. Fang, P.Jarillo-Herrero, and E. Kaxiras, Phys. Rev. B **98**, 085144 (2018).
- [9] C.A. Santini *et al.*, Nature Communications **6**:8600, 1 (2014).
- [10] A.J.J. van Dalen, R. Griessen, S. Libbrecht, Y. Bruynseraede, and E. Osquiguil, Phys. Rev. B **54**(2), 1366 (1996).
- [11] N. Gheorghiu, C.R. Ebbing, B.T. Pierce, and T.J. Haugan, arXiv:1909.12145 (2019) and as IOP Proceedings paper for CEC-ICMC 2019 (to be published).
- [12] M. Kühne *et al.*, Nature **564**, 235 (2019).
- [13] H.K. Henish, Mat. Res. Bull., textbf24, 749 (1989).
- [14] B. Standley, A. Mendez, E. Schmidgall & M. Bockrath, Nano. Lett. **12**, 1165 (2012).
- [15] M.S. Dresselhaus, G. Dresselhaus, K. Sugihara, I.L. Spain, and H.A. Goldberg, *Graphite Fibers and Filaments* (Springer-Verlag, 1988).
- [16] J. Shen, Z. Chen, N. Wang, W. Li, and L. Chen, Appl. Phys. Lett. **89**, 153132 (2006).
- [17] Z. Xu, Z. Liu, H. Sun, and C. Gao, Adv. Mater. **25**, 3249 (2013).
- [18] C. Subramaniam, T. Yamada, K. Kobashi, A. Sekiguchi, D.N. Futaba, M. Yumura & K. Hata, Nat. Commun. **4**:2202 (2013).
- [19] G.E. Pike, A.W. Mullendore, J.E. Schirber, and J. Napier, IEEE Transactions on Magnetism, vol. **MAG-11**, no. **2**, 185 (1975).
- [20] V.M. Pathare and J.W. Halloran, *Electrical superconducting ceramic fiber devices*, US Patent 4990490 A (1991).
- [21] M. Dietrich, C.-H. Dustmann, F. Schmaderer, G. Wahl, IEEE Transactions on Magnetism, Vol. **MAG-19**, No. **3**, 406 (1983).
- [22] T. Haugan, P.N. Barnes, R. Wheeler, F. Meisenkothen, M. Sumption, Nature **430**, 867 (2004).
- [23] S. Ono, Y. Toda, and J. Onoe, Phys. Rev. B **90**, 155435 (2014).
- [24] B.T. Pierce, J.L. Burke, L.B. Brunke, T.J. Bullard, D.C. Vier, and T.J. Haugan, IEEE Transactions on Applied Superconductivity **23**(3), 7000205 (2013).
- [25] www.cyttec.com
- [26] U. Nandi, D. Jana, and D. Talukdar, Progress in Material Science **71**, 1 (2015).
- [27] Y. Kawashima & M. Iwamoto, Sci. Rep. **6**, 28493 (2016).
- [28] Y. Kawashima, arXiv:1612.05294 (2016).
- [29] Lake Shore Cryogenics, Inc., www.lakeshore.com
- [30] J.W. Ekin, *Experimental Techniques for Low-temperature Measurements* (Oxford University Press, 2006).
- [31] Everett Charles Technologies Inc., www.ectinfo.com
- [32] W. Norimatsu, T. Maruyama, K. Yoshida, K. Takase, and M. Kusunoki, Appl. Phys. Express **5**, 105102, (2012).
- [33] H. Kempa, P. Esquinazi, and Y. Kopelevich, Solid State Commun. **138**(3), 118 (2006).
- [34] Y. Kopelevich, B. Raquet, M. Goiran, W. Escoffier, R.R. daSilva, J.C. MedinaPantoja, I.A. Lukyanchuk, A. Sinchenko, P. Monceau, Phys. Rev. Lett. **103**, 116802 (2009).
- [35] E. Dagotto, Science **293**, 2410 (2001).
- [36] I. Tamir, A. Benyamini, E.J. Telford, F. Gorniaczyk, A. Doron, T. Levinson, *et al.*, Sci. Adv. **5**:eaau3826, 1 (2019).
- [37] M. Tinkham, Phys. Rev. Lett. **61**, 1658 (1988).
- [38] J.S. Langer and V. Ambegaokar, Phys. Rev. **164**, 498 (1967); D.E. McCumber and B.I. Halperin, Phys. Rev. B **1**, 1054 (1970).
- [39] H. Zhan, G. Zhang, V.B.C. Tan, Y. Cheng, J.M. Bell, Y.-W. Zhang, and Y. Gu, Adv. Funct. Mater. **26**, 5279 (2016).
- [40] V.Z. Kresin, V.A. Litovchenko and A.G. Panasencko, J. Chem. Phys. **63**, 3613 (1975).
- [41] A. Mourachkine, *Room-Temperature Superconductivity* (Cambridge International Science Publishing, 2004).
- [42] M.M. Dejev, I.V. Klimenko, and T.S. Zuravleva, Synthetic Metals **71**, 1769 (1995).
- [43] R.A. Davison, K. Schalm, and J. Zaanen, Phys. Rev. B **89**, 245116 (2014).
- [44] E.H. Hwang and S. Das Sarma, Phys. Rev. B **99**, 085105 (2019).
- [45] D. A. Balaev, S. I. Popkov, K. A. Shakhutdinov, and M. I. Petrov, Physics of the Solid State, **48**(5), 826 (2006).
- [46] T.W. Barbee III, A. Garcia & M.L. Cohen, Nature textbf340. 369 (1989).
- [47] K.A. Johnson & N.W. Ashcroft, Nature **403**, 632 (2000).
- [48] C.F. Richardson and N.W. Ashcroft, Phys. Rev. Lett. **78**(1), 118 (1997).
- [49] Y. Gefen, W.-H. Shih, R.B. Laibowitz, and J.M. Viggiano, Phys. Rev. Lett. **57**(24), 3097 (1986).
- [50] J. Ruvalds, Supercond. Sci. Technol. **9**, 905 (1996).
- [51] D. Bercioux, T.M. Klapwijk, and F.S. Bergeret, PRL **119**, 067001 (2017).
- [52] N. Gheorghiu, C.R. Ebbing, and T.J. Haugan, arXiv:2005.05876v1 (2020).
- [53] G.-. Zhao, preprint cond-mat/0208200 (2000).
- [54] M. Silaev, Phys. Rev. B **99**(22), 224511 (2019).
- [55] C. Eistrup, C. Walsh and E.F. van Dishoeck, Astronomy & Astrophysics **629**, A84 (2019).
- [56] D.V. Kveshchenko, J. Phys.: Condes. Matter **21**, 075303 (2009).
- [57] N. Garcia, P. Esquinazi, J. Barzola-Quiquia, and S. Dusari, New J. of Phys. **14**, 053015 (2012).
- [58] A. Ballestar, T.T. Heikkilä, and P. Esquinazi, Supercond. Sci. Technol. **27**, 115014 (2014).
- [59] P.A. Heiney, J.E. Fischer, A.R. McGhie, W.J. Romanow, A.M. Denenstien, J.P. McCauley, Jr., A.B. Smith, D.E. Cox, Phys. Rev. Lett. **66**(220), 2911 (1991).
- [60] E. Grivei, M. Cassart, J.P. Issi, L. Langer, B. Nysten, J.P. Michenaud, C. Fabre, and A. Rassat, Phys. Rev. B. **48**(11), 8514 (1993).
- [61] A. Szasz, Journal of Superconductivity, **6**(2), p. 99 (1993).
- [62] V. Kresin, J Supercond Nov Magn **25**, 711 (2012).
- [63] I. Bozovic, G. Logvenov, I. Belca, B. Narimbetov, and I. Sveklo, Phys. Rev. Lett. **89**(10), 107001 (2002).
- [64] D. Pelc, M. Vučković, M.S. Grbić, M. Pozek, G. Yu, T. Sasagawa, *et al.*, Nature Communications **9**:4327, 1 (2018).
- [65] Y.-Z. Chou, Y.-P. Lin, S. Das Sarma, and R.M. Nandkishore, Phys. Rev. B **100**, 115128 (2019).
- [66] J.C. Phillips, Proceedings of SPIE Vol. 4058, 371 (2000).
- [67] P.D. Esquinazi, C.E. Precker, M. Stiller, T.R.S. Cordeiro, J. Barzola - Quiquia, A. Setzer, and W. Böhlmann, Quantum Stud.: Math. Found., 1 (September 9, 2017).

- [68] T.T. Heikkilä and G.E. Volovik, *Flat bands as a route to high-temperature superconductivity in graphite*, in book: *Basic Physics of Functionalized Graphite*, ed. P. Esquinazi (Springer, 2016).
- [69] G.T. Stewart, *Liq. Cryst.* **31**(4), 443 (2004).
- [70] T.P. Fraccia, G.P. Smith, M. Todisco, G. Zanchetta, N.A. Clark and T. Bellini, XVIII-th Intl. Conf. on Origin of Life (San Diego, 2017).
- [71] A.R. Sarafian, S.G. Nielsen, H.R. Marschall, F.M. McCubbin, and B.D. Monteleone, *Science* **346**(6209), 623 (2014).
- [72] J. Ladik and A. Bierman, *Phys. Lett.* **29A**(10), 636 (1969).
- [73] V.D. Lakhno and V.B. Sultanov, *J. Appl. Phys.* **112**, 064701 (2012).
- [74] G. Stando, D. Lukawski, F. Lisiecki, and D. Janas, *Applied Surface Science* **463**, 227 (2019).
- [75] V.L. Ginzburg, *Phys. Lett.* **13**(2), 101 (1964).
- [76] Y. Tada, *Phys. Rev. B* **97**, 014519 (2018).
- [77] A. Salam, *Phys. Lett. B* **288**, 153 (1992).
- [78] K.H. Johnson, *Physica C: Superconductivity and its applications* **547**, 55 (2018).
- [79] R.M. Khusnutdinoff and A.V. Mokshin, *Journal of Crystal Growth* **524**, 125182 (2019).
- [80] R. Franklin and R.G. Gosling, *Acta Cryst.* **6**, 673 (1953); J.D. Watson and F.H.C. Crick, *Nature* **171**, 737 (1953); J.D. Watson, *Nature* **422**, 809 (2002); W. Fuller, *Nature* **424**, 876 (2003).
- [81] E.F. Sheka & N.A. Popova, *J Mol Model* **18**, 3751 (2012); E.F. Sheka, N.A. Popova, V.A. Popova, *Physics - Uspekhi* **61**(7), 645 (2018).
- [82] P. Mikheenko, *J Superconduct Novel Magn* **32**, 1121 (2019).
- [83] W.A. Little, *Phys. Rev.* **134**, A1416 (1964).
- [84] J.R. Schrieffer, *J Superconduct: Incorporating Nov Magn*, **17**(5), 539 (2004).